Widening the bandgap of phonon crystal through its structure parameter optimization

Khemrith Bun[2], Saurabh Pathak [1,2] and Xu Wang[2,]*

[1] Department of Mechanical Engineering, University of Melbourne, Parkville, VIC, 3010 Australia

[2] School of Engineering, RMIT University, Australia

***Corresponding Authors:** xu.wang@rmit.edu.au*

Abstract

The increasing demand for renewable energy and shortage of resources in today's world has been stimulating researchers to explore means for the extraction of energy from wasted heat sources. Thermoelectric materials can convert thermal energy directly into electric energy and vice versa. In this paper, a phonon crystal structure has been proposed and characterized to study its bandgap magnitude and the effect on the thermal conductivity which could increase the efficiency of the thermoelectric materials. The novelty of this paper is the phonon crystal structure that has been proposed and the method to study the effects of different dimensional parameters of the phonon crystal structure on the bandgap magnitude. The phonon crystal's bandgap is simulated by the COMSOL software and then validated with other literature results. Based on the validated simulation model, a regression parameter model is developed from the COMSOL software simulation. The model is used to predict the magnitude of the bandgap of the phonon crystal structure from input design parameters where the sensitivity of the design parameters and their interactions can be analyzed. The design parameters can be optimized for the biggest bandgap magnitude based on the regression parameter model. The optimization results show a significant improvement in the magnitude of the bandgap.

I.Introduction

Increasing energy efficiency is demanded as energy consumption increases in various applications such as transportation, businesses, and industries. The use of non-renewable energy resources has been increased to meet energy demands but at a cost of increased greenhouse emissions and environmental pollution which lead to global warming. Much interest has been shown in utilizing waste heat recovery methods to increase the thermal efficiency to meet the miscellaneous energy demands rather than the use of additional non-renewable energy resources. [1] Thermoelectric materials, as a potential candidate for the direct interconversion of thermal and electrical energy, have attracted considerable attention in the field of energy harvesting and thermal management applications. The electricity generation from waste heat via thermoelectric

devices can be considered a new energy source. For instance, automotive exhaust gas and all industrial processes generate an enormous amount of waste heat that can be converted to electricity by using thermoelectric devices. [2]

The efficiency of thermoelectric materials can be well quantified by the dimensionless figure of merit, ZT as shown in Eq. (1).

$$ZT = \frac{\sigma S^2 T}{\kappa} \tag{1}$$

where σ is the electrical conductivity, S is the Seebeck coefficient, T is the temperature and κ is the thermal conductivity. The high figure of merit is hindered by the high thermal conductivity of the material. [3] The increase in the phonon wave activity greatly influences the thermal conductivity, and dispersion of this wave activity improves the thermoelectric efficiency of the material. One effective way of lowering the thermal conductivity is to introduce holes in the lattice and create a phonon crystal. [4] The structure with a periodic arrangement of holes in it is called a phonon crystal. One challenge when building a phonon crystal is to try to keep the electrical conductivity high at the same time. Often when phonon crystals are created both the thermal and electrical conductivity is lowered, which is not optimal. [5] If the material is selected and constructed correctly and the phonon wave dispersion is high, the thermal conductivity will be lowered much more than the electrical conductivity. This is possible as the electrical conductivity is likely to be lowered due to the removal of material. [6] Optimization of band gap structures or phonon crystals has seen an increase in interest over the last decade. [7] The topic is challenging owing to the wide applicability of the metamaterials featured by the band gap property. Moreover, new technologies like 3D printing show new perspectives on the optimal metamaterial design based on computational analysis. [8]

A band gap means that phonons of certain frequencies cannot propagate through the medium.[9] Gaps may appear in the wave frequency band structure for periodic materials implying that waves cannot propagate in certain frequency ranges. If the conditions for wave interference are satisfied, periodic structures that possess phononic bandgaps can block or reflect heat. [10] If a thermal vibration (with its frequency in the thermal frequency gap) is generated within the system, it will be blocked irrespective of its propagation direction. [11] The medium can be modified to create or suppress band gaps. The modification can be done by introducing defects like holes in the lattice. [12]

In this paper, a novel phonon crystal structure has been proposed and characterized to study its bandgap magnitude response to different geometrical and dimensional parameter changes. Three geometrical and dimensional parameter inputs of the novel phonon crystal will be selected and defined. The effect of each parameter will be quantified and compared using the response surface method (RSM). The RSM tool is applied to optimize the input parameters for the largest bandgap in this study. The sensitivity of the parameters and their interactions also has been analyzed. The parameters have been optimized for the largest bandgap magnitude possible. The optimal combination of the parameters has been compared with and verified by the result obtained solely on COMSOL simulation software. The COMSOL model simulation results are compared with the results obtained from an already published paper to validate the COMSOL model. Different geometries are tested to see how they affect the magnitude of the bandgap. With the optimal geometrical and dimensional parameter combination that produces the biggest bandgap magnitude, the thermal conductivity of the phonon crystal can be greatly reduced, hence resulting in an increase in thermoelectric efficiency.

II. Finite element analysis modelling and validation

Eigen analysis of basic topologies of periodic structures can be used as a systematic approach to identify mode frequency and shapes of unit cells and their basic mode mechanisms. [13] The eigenmode shapes from this analysis display all possible unit cell mode shapes derived from a basic unit cell while guaranteeing that the resulting cell mode shapes can be arranged in a periodic lattice. The crystal structure of an infinite silicon lattice was modelled based on the finite element analysis simulation model in the COMSOL Multiphysics software using the Floquet boundary conditions (Floquet BC) [14]. As shown in Fig. 1, the model is a two-dimensional square structure where holes are introduced to study the band structure. It will be built using Solid mechanical structure physics and Eigen frequency solver study. The model is built using only the unit cell for the structure. Figure 2 shows the resulting unit cell when modelled in COMSOL. The lattice constant size, the size of the holes and the cell's thickness could be changed/modified to affect the magnitude of the bandgap. The lattice constant is defined as the distance "*a*" between two centers of the two adjacent circular holes. "*D*" is the diameter of the holes. "*b*" is the side length of the unit cell, the distances between the two edges of the two adjacent holes as shown in Figure 2.

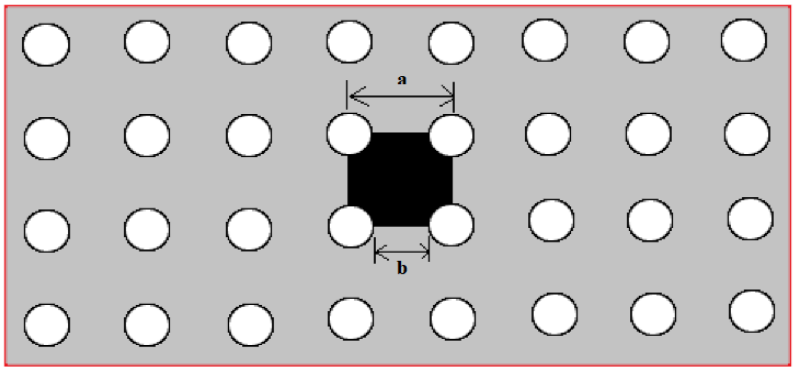

Figure 1 A two-dimensional crystal model of periodical structures with a unit cell in the lattice.

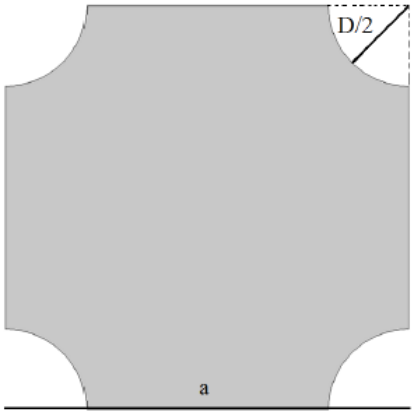

Figure 2 A square lattice unit cell with holes on the edge.

After the model is generated, materials were chosen and applied to the model. The material of the solid medium chosen for the model is pure silicon and the material of the holes is air. It is assumed that the silicon material in the simulation is orthotropic rather than isotropic since this assumption reflects the real-life situation better. [15] The material properties of the orthotropic silicon are shown in Table 1. The mesh size "Coarser" was chosen after the convergence test is carried out. A finer mesh than this is unnecessary as it does not increase the accuracy and will take a much longer computational time. [16]

Table 1. Material properties used for the orthotropic silicon in the literature [14]

Direction	X	Y	Z

Young's modulus [GPa]	169	169	130
Poisson's ratio (Dimensionless)	0.064	0.28	0.36
Shear modulus [GPa]	50.9	79.6	79.6

Floquet-type boundary conditions can be applied to compute eigenfrequencies for a large repetitive grid using a model containing only a unit cell. Floquet boundary conditions were selected and applied to the model with the wave number vectors K_x and K_y along the x and y directions of the model as shown in Figure 3. In these boundary conditions, the wave vectors *Kx* and *Ky* are used to define the periodic condition within the first Brillouin Zone. The two periodic conditions are shown with the red lines for the x-direction and the blue lines for the y-direction. The Floquet boundary condition for an infinite-plate waveguide can be expressed and given by

$$u_{destination} = u_{source} \cdot e^{-ik_F(r_{destination} - r_{source})} \quad (2)$$

where k_F is the Floqent wavenumber, *u* is the displacement field and *r* is the spatial coordinate of the boundaries where it is applied. The source and destination are applied once to the left and right edges (red lines) of the unit cell for x-direction and once to the bottom and top edge (blue lines) for y-direction.

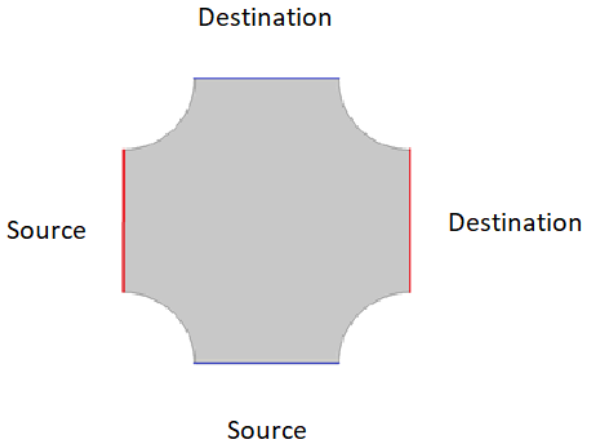

Figure 3. The boundary conditions for the unit cell

The model settings are Eigen frequency and parametric sweep of parameter 'k' with an increment of 0.1 with a range of 0 to 3 which sweeps over the total billion zones varying the wave number vectors K_x and K_y with every increment of parameter k. When k is between 0 and 1 it corresponds to the MΓ direction and both K_x and K_y wave number vectors were varied from 0 to $\frac{\Pi}{a}$. When k is between 1 and 2 it corresponds to the ΓX direction and K_y is 0 and K_x is carried from 0 to $\frac{\Pi}{a}$. The last direction XM is when k is between 2 and 3 and K_x is fixed at $\frac{\Pi}{a}$ and K_y wavenumber is varied from 0 to $\frac{\Pi}{a}$. The parametric sweep parameter 'k' could be summarized in Fig. 4.

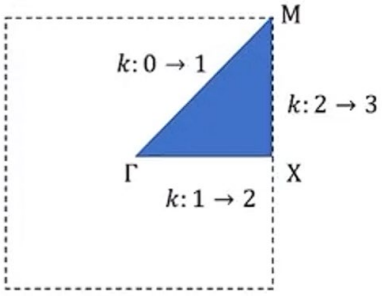

$$K_x = \begin{cases} (1-k)\frac{\Pi}{a}\ ; 0 < k < 1 \\ (k-1)\ \frac{\Pi}{a}\ ; 1 < k < 2 \\ \frac{\Pi}{a}\ ; 2 < k < 3 \end{cases} \qquad K_y = \begin{cases} (1-k)\frac{\Pi}{a}; 0 < k < 1 \\ 0\ ; 1 < k < 2 \\ (k-2)\frac{\Pi}{a}; 2 < k < 3 \end{cases}$$

Figure 4 Symmetry points of the Lattice and the given vectors directions of M to Γ, Γ to X, and X to M with their limits

The obtained band structure results are visualized with a 2-dimensional plot group with an x-axis containing all values of wave number vector 'k' and the y-axis containing the wave

frequency of the solid medium with a unit of Hz. Wave number vector of 0 to 1 shows the vector directions of M to Γ, wave number vector of 1 to 2 show the vector direction of Γ to X and wave number vector of 2 to 3 shows the vector direction of X to M. For each parameter, we solve for the selected lowest natural frequencies for the first 8 eigenfrequencies. We then plot the wave propagation frequencies versus each value of "*k" between 0 to 3 with an increment of 0.1* for different dispersion curves along different vector paths/directions. A band gap appears in the plot as a region in which no wave dispersion curves exist. The largest frequency band gap range is recorded along with its magnitude as shown in Figure 5.

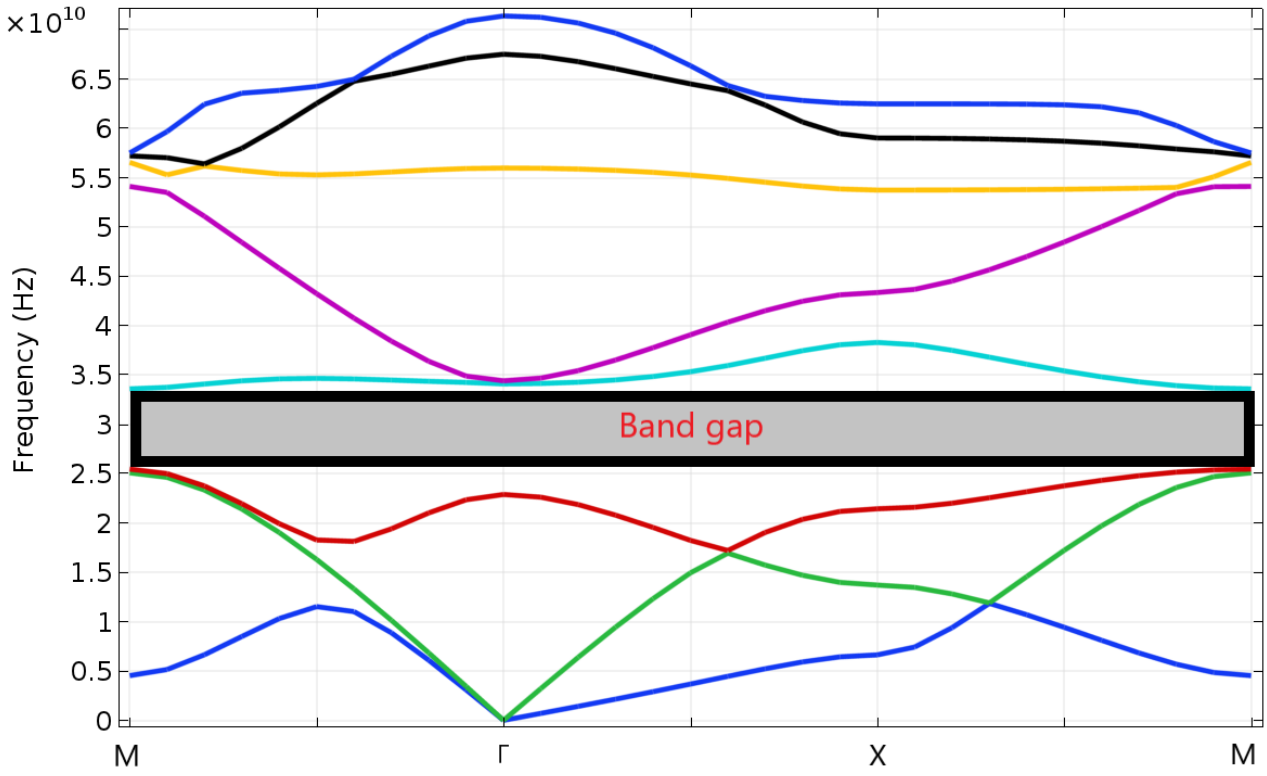

Figure 5. The phonon wave dispersion curves (wave frequency (Hz) versus the wave number (*k*) and the bandgap magnitude.

III.Model validation

The COMSOL simulation model used in this study is validated with the model from the previously published works found in the literature [11-12,15-16] where the results as presented in

Figures 6-9. The wave vector setup in the literature's model will be applied in our COMSOL model set up to calculate the phonon wave dispersion curves and the magnitude of the maximum bandgap. All the comparisons are based on a single unit cell square lattice structure model. The model that is used for our study will have the same wave number vector (k_x and k_y), boundary condition, and parametric increment of "k" as those of the literature's model. The results are compared to verify the accuracy of the models. The model has also been validated in different studies such as electromagnetic wave study and acoustic pressure wave study [17] that are used to calculate the eigenfrequencies instead of solid mechanics wave study. These parameters for the boundary conditions could only be transferrable between the models only when the wave number vectors are correctly set up.

Figure 6 is taken from the literature [18] and shows the phonon wave dispersion curves for a silicone structure with air holes of 90 nm diameter. Figure 6 also shows the simulated version using the Solid mechanic study for the same structure.

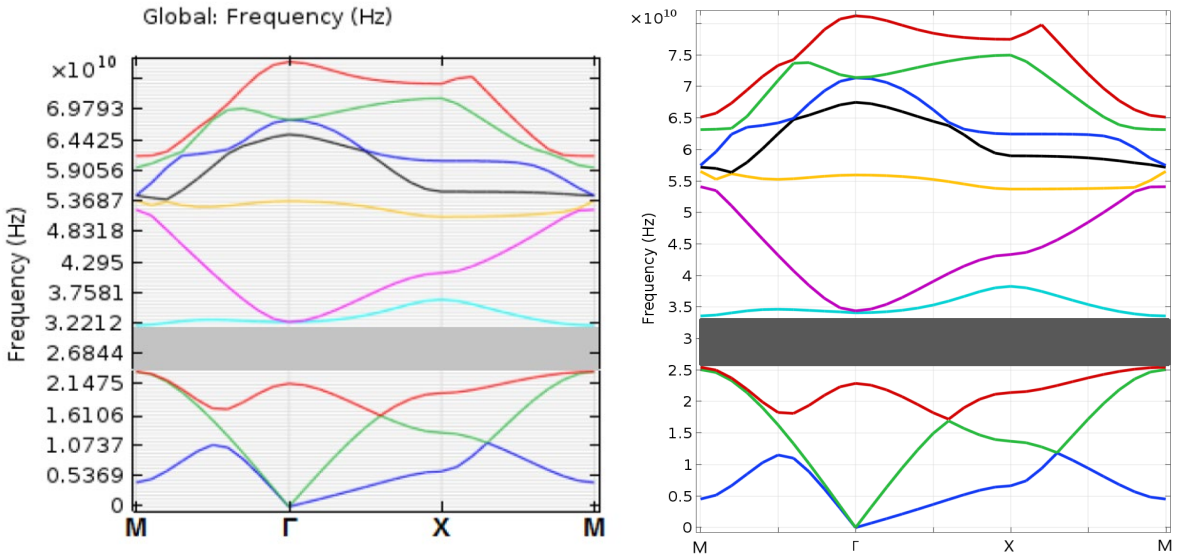

Figure 6. Wave dispersion curves and band structure for silicone unit cell structure with circular holes of D=90 NM, a=100 NM from Literature [18] (Left), and our COMSOL model simulation (Right).

Figure 7 is taken from the literature [17] and shows the wave dispersion curves and their band structure of a simple two-dimensional (2D) photonic crystal. The photonic crystal consists of a vacuum square lattice with dielectric rods which are transverse magnetic polarization with an electric field along the rod axis. The photonic crystal is used for the study of electromagnetic wave propagation while the phonon crystal is used for the study of the acoustic wave counterpart [19].

The model used for the study of the electromagnetic wave has the electric field components solved for out-of-plane vector using the wave equation for refractive index. In the model, the lattice constant is "*a*", the radius is set at $R = 0.2a$, the speed of light is "*c*", the relative permittivity is $\varepsilon = 12.5$, and permeability $u = 1$.

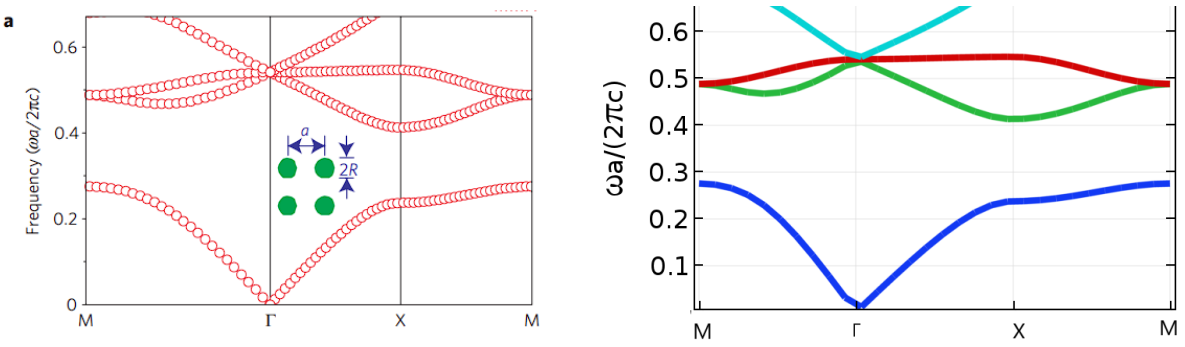

Figure 7. The wave dispersion curves and their band structure for a 2-dimension photonic crystal (PC) which was constructed of cylinders with lattice constant a=1 mm and radius R=0.2 mm and dielectric properties of relative permittivity $e = 12.5$ and permeability u =1 from the literature [17] (Left) and from our COMSOL simulation model (Right).

Figure 8 is taken from the literature [11] and shows the wave dispersion curves and their band structure of a phonon crystal including the cylindrical polyvinylchloride (PVC) pipe in the air. In the phonon crystal, the diameter of the cylindrical polyvinylchloride (PVC) pipe is $D = 25.8$ mm and the lattice constant or the center-to-center distance between lattice points is $a = 27$ mm. Material properties including mass densities, longitudinal elastic wave speed, and transversal elastic wave speed in the PVC and air structure are given in Table 2. It is assumed that the PVC cylinders are infinitely rigid in the out-of-plane direction. An acoustic pressure wave study is conducted in the frequency domain using a linear elastic wave model with specific mass density and speed of sound.

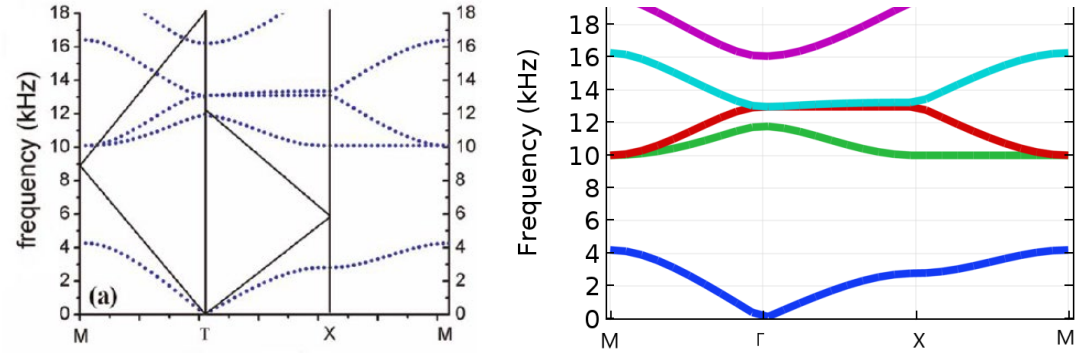

Figure 8. The wave dispersion curves and their band structure for the PVC pipe with a diameter of 25.8 mm and lattice constant a = 27 mm in the air matrix from the literature [11] (Left) and our COMSOL simulation model (Right).

Table 2. A material property of the polyvinylchloride (PVC) and air in the phonon crystal [11].

Material	Density (kg/cm^3)	longitudinal Wave speed (m/s)	Transversal Wave speeds (m/s)
PVC	1364	2230	1000
Air	1.3	340	0

Figure 9 is taken from the literature [12]. The numerical setups of the simulation model are similar to those of the previous literature [11]. The phonon crystal system comprises steel scatterers embedded in the air where the diameter of the steel cylinder is D = 22 mm and the lattice constant is a = 6.5 mm. Material properties including the mass density and velocities of the sound in the steel and air are given in Table 3.

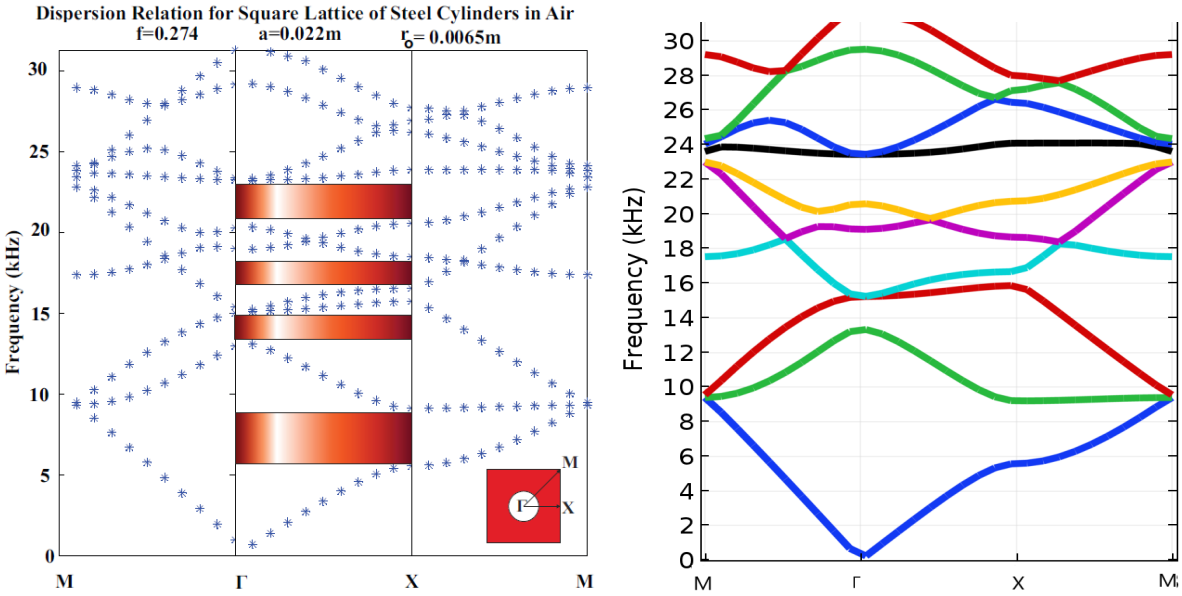

Figure 9. The wave dispersion relation curves of a phonon crystal consisting of the steel scatterers embedded in the air (a = 22 mm, r = 6.5 mm) from the literature [12] (Left) and from our COMSOL simulation model (Right).

Table 3. Material properties used for the steel and air in the phonon crystal [12]

Material	Density kgm^{-3}	The velocity of Sound ms^{-1}
Steel	7800	6100
Air	1.2	343

IV. Response surface model of the maximum bandgap of a unit cell

The bandgap magnitude of a unit cell can be related to three system geometrical and dimensional property parameters: the lattice constant, the side length (hole's radius), and the thickness. The lattice constant is the side length of the whole square including the hole areas within the whole square area. The unit cell side length is the lattice constant minus the hole diameter. The thickness is the thickness of the unit cell. The variation ranges of the parameters are shown in Table 4.

Table 4. The parameter variation ranges.

Parameter	**Variation Range**
Side Length z_1 (nm)	10-20
Lattice Constant z_2 (nm)	100-150
Thickness z_3 (nm)	1-5

These parameters have a direct impact on the bandgap magnitude which will be considered as the response target and will be adjusted in their variation ranges to achieve the maximum bandgap magnitude. The input parameters are arranged in the orthogonal central composite design (CCD) to develop the response surface method (RSM) parameter regression prediction model of the maximum bandgap magnitude of the square lattice unit cell from the input geometry design parameters where the sensitivity of the maximum bandgap magnitude to the input geometry design parameters and their interactions can be analyzed. This model can be used to define the interrelations between the input geometry parameters (the studied variables), and to describe the combined effect of all factors with a minimum number of experiments needed to be conducted.

The non-linear relationship model between the input parameter and output bandgap magnitude can be obtained from the CCD design of the input parameters and corresponding bandgap magnitude values presented in Table 5 using RSM where the corresponding bandgap

magnitude values are predicted from the validated COMSOL simulation model. The RSM model can be applied to analyze the sensitivity of the target bandgap magnitude to the input geometry design parameters and their interactions. The RSM model can also be used to predict any target output response value from any input geometry design parameters within their pre-specified variation ranges and to optimize the input geometry design parameters for the maximum bandgap magnitude.

Table 5. The dimensionless and actual dimensional input parameter values in the CCD design.

Parameter	x_i (-1.31607)	x_i (-1)	x_i (0)	x_i (1)	x_i (1.31607)
z_1: Side Length (nm)	8.419	10	15	20	21.580
z_2: Lattice Constant (nm)	92.098	100	125	150	157.902
z_3: Thickness (nm)	0.3678	1	3	5	5.632

Table 6 Sixteen sets of experimental runs with different combinations of the dimensionless input parameters and corresponding bandgap magnitude predicted from the COMSOL simulation

			Bandgap Magnitude (GHz)	
x_1: Gap Radius	x_2: Lattice Constant	x_3: Gap Radius	COMSOL	RSM
-1	-1	-1	8.13	8.0297
1	-1	-1	3.67	3.7695
-1	1	-1	5.97	5.8809
1	1	-1	5.25	5.3607
-1	-1	1	3.64	3.5409
1	-1	1	1.64	1.7407
-1	1	1	2.6705	2.5825
1	1	1	2.345	2.4567
-1.31607	0	0	4.118	4.421701
1.31607	0	0	2.519	2.215172
0	-1.31607	0	5.14	5.142113
0	1.31607	0	16.34	16.35506
0	0	-1.31607	10.43	10.43188
0	0	1.31607	3.171	3.167148
0	0	0	4.34	4.34
0	0	0	4.34	4.34

A total of 16 sets of input dimensionless parameter combinations are designed according to the CCD design of input parameters as shown in Table 6 to develop the RSM model where

α=1.31607 is the star value. x_i (i=1-3) is the dimensionless input parameter that changes from -1 to +1 corresponding to the dimensional input parameters z_i (i=1-3) which changes from the minimum to maximum values. The dimensional input parameters z_i (i=1-3) can be converted into the dimensionless input parameters x_i (i=1-3) by the following equation.

$$\begin{cases} z_0 = \dfrac{z_{\max} + z_{\min}}{2} \\ \Delta z = \dfrac{z_{\max} - z_{\min}}{2} \\ x_i = \dfrac{z_i - z_0}{\Delta z}; \quad i=1,2,3 \end{cases} \tag{2}$$

It was found from Table 6 that the bandgap magnitude results range from 1.64 to 16.34 GHz with different parameter combinations. The highest bandgap magnitude of 16.34 GHz is obtained with a side length of 15 nm, a lattice size of 157.902 nm, and a thickness of 3 nm.

The relationship between the input variables and target response can be approximated in a non-linear polynomial equation and given by

$$\tilde{Y} = \beta_0 + \sum \beta_i x_i + \sum \beta_{ii} x_i^2 + \sum \beta_{ij} x_i x_j + \cdots + \varepsilon \tag{3}$$

RSM model is developed from the CCD arranged input parameters and corresponding response targets calculated from the simulated results of the COMSOL model which are listed in the second last column of Table 6.

The mathematical expression of the regression parameter model for the prediction of the bandgap magnitude can be developed and shown in Equation (4). In this equation, the coefficient amplitude or its absolute value of each equation term has quantified the magnitude of the effect of that specific parameter on the bandgap magnitude. The positive and negative signs represent the positive effect and negative effect, respectively. Therefore, it is concluded that the x_2 lattice size and x_3 thickness have the largest and second-largest positive effect on the bandgap magnitude, while the x_1 side length has the least effect on the bandgap magnitude. In Equation (4), the coefficient magnitudes of the term x_1x_2, x_1x_3, and x_2x_3 represent the interaction effect magnitudes of two of the three parameters on the bandgap magnitude. It is seen from Equation (4) that x_1x_2 has a larger positive effect than x_1x_3 and x_2x_3. The parameter x_2 gives the largest coefficient absolute value of 4.26. The parameter x_1 has the least effect on the bandgap magnitude of only -0.838 as shown in Equation (4) which is given by

$$\textit{The maximum bandgap magnitude (THz)} = 4.34 - 0.8383x_1 + 4.26x_2 - 2.76x_3 + 0.6768x_1x_2 + 0.3568x_1x_3 + 0.0394\,x_2\,x_3 - 0.5898\,x_1^2 + 3.7x_2^2 + 1.42x_3^3 - 0.2582x_1x_2x_3 + 1.17\,x_2^2x_3 - 4.36\,x_2x_3^2 - 4.7\,x_2^2x_3^2 \quad (4)$$

Table 7 The ANOVA *F*-value and *P*-value against each term

Source	Sum of squares	d*f*	Mean square	*F*-value	*p*-value	R^2: 0.9987 Adjusted R^2: 0.99
Model	206.31	13	15.87	120.06	0.0083	significant
x_1 Side Length	8.06	1	8.06	60.94	0.0160	significant
x_2 Lattice Constant	62.72	1	62.72	474.49	0.0021	significant
x_3 Thickness	26.35	1	26.35	199.32	0.0050	significant
$x_1\,x_2$	3.66	1	3.66	27.72	0.0342	significant
$x_1\,x_3$	1.02	1	1.02	7.71	0.1090	
$x_2\,x_3$	0.0124	1	0.0124	0.0941	0.7880	
x_1^2	1.04	1	1.04	7.89	0.1068	
x_2^2	40.96	1	40.96	309.87	0.0032	significant
x_3^2	6.05	1	6.05	45.80	0.0211	significant
$x_1\,x_2\,x_3$	0.5333	1	0.5333	4.03	0.1823	
$x_2^2\,x_3$	3.29	1	3.29	24.92	0.0379	significant
$x_2\,x_3^2$	45.97	1	45.97	347.75	0.0029	significant
$x_2^2\,x_3^2$	24.75	1	24.75	187.26	0.0053	significant

The RSM model of Equation (4) can be validated by the analysis of variance (ANOVA). The results of the ANOVA are shown in Table 7. The *P*-value of the ANOVA needs to be less than 0.05 which represents that there is less than a 5% chance that the corresponding *F*-value could occur due to noise. The *P*-value is less than 0.05 indicating the model term is significant. The *F* value is used to measure the significance of the overall ANOVA model where a higher *F* value indicates a more accurate and reliable model. For the RSM model to be accurate and significant, the *P*-value needs to be kept less than 0.05 while the *F*-value should be maintained as high as possible. The *F*-value of the RSM model is as high as 120.06 and the *P*-value is less than 0.0083,

which means that the RSM model is significant with an accurate and reliable prediction. Moreover, the coefficient R^2 and adjusted R^2 of the presented RSM model are 0.9987 and 0.99. A value of the coefficient R^2 and adjusted R^2 close to 1 indicates good model accuracy which has further validated the RSM model from a statistical perspective.

Additionally, the sensitivity of the response target on input parameters can also be validated by assessing the F values and P-values of the individual equation terms as shown in Table 7. [20] According to Table 7, the F values of the term x_2 (lattice constant) of 474.49 and terms x_3 (thickness) of 199.32 are the largest and second largest among those of all the three parameters. The F value of x_1 (side length) of 60.94 is the smallest. x_1 has the least effect on the bandgap magnitude among all the three individual parameters. x_2 has the largest effect on the bandgap magnitude. These conclusions have validated the conclusions of the sensitivity of the individual terms and coupling terms derived from the coefficients of Equation (4). This means that sensitivities of the response target of the maximum bandgap magnitude on input parameters can also be assessed from the ANOVA results.

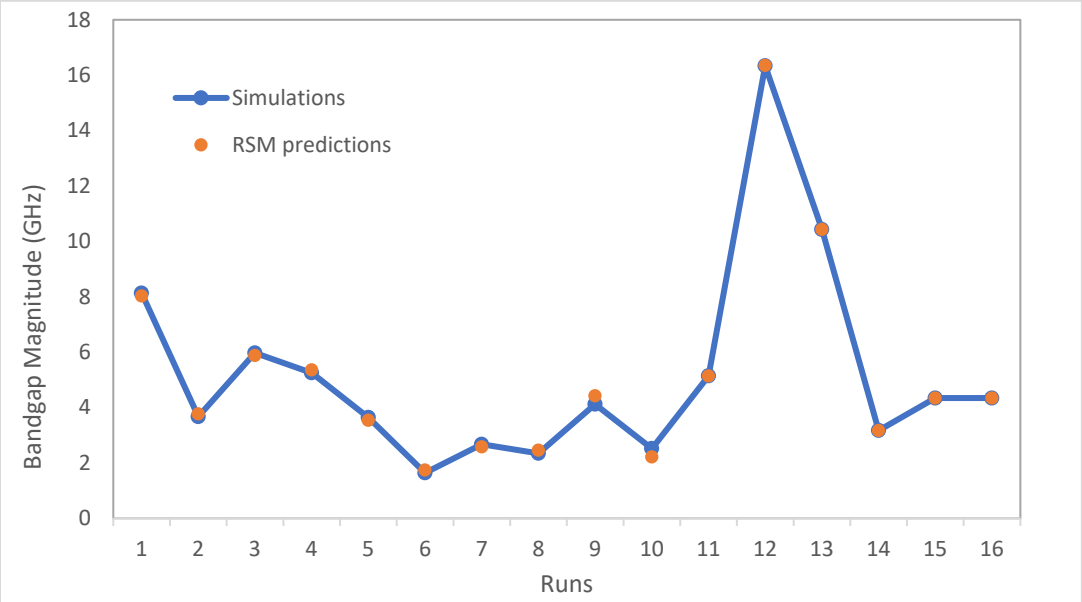

Figure 10. The comparison of the bandgap magnitude (GHz) was calculated from the COMSOL simulation model and from Equation (4).

Shown in Fig. 10 is the comparison of the COMSOL simulation results of the response target of the maximum bandgap magnitude values which are listed in the second last column of Table 6 and the prediction results of the response target of the maximum bandgap magnitude values calculated by Equation (4) from the 16 sets of input parameters in Table 6. The prediction

results of the response target of the maximum bandgap magnitude values calculated by Equation (4) are listed in the last column of Table 6. It is shown that the results calculated by Eq. (4) are very close to those of the COMSOL simulation model. In other words, the results in the last two columns of Table 6 are very close, which has validated Equation (4) for the bandgap magnitude prediction.

The dimensionless boundary range of all the input parameters from -1 to 1 indicates all the parameters vary between their minimum value and maximum value. Within this range, the predicted maximum bandgap magnitude value obtained from Equation (4) is 16.355 GHz with a parameter combination of the side length of 15.268 nm, the lattice constant of 157.889 nm, and the thickness of 2.933 nm, which is higher than the CCD result 16.34 GHz of the optimal parameter combination of the side length of 15 nm, the lattice constant of 125 nm and the thickness of 3 nm as shown in Table 6.

The effects of input parameters on the maximum bandgap magnitude have been quantified based on the absolute value magnitudes of the coefficients of the individual terms of Equation (4). The sensitivity of the maximum bandgap magnitude to input parameters is presented in Figure 11. It is shown from Figure 11 that the input parameter of the largest effect is the lattice constant. The parameter has a positive effect on the maximum bandgap magnitude. This means that increasing the lattice constant will increase the maximum bandgap magnitude. The thickness parameter has the second-largest effect and has a negative effect. This means that decreasing the thickness will increase the maximum bandgap magnitude. The side length has the least effect on the maximum

bandgap magnitude. Therefore, the most efficient way to increase the maximum bandgap magnitude is to increase the lattice constant as large as possible and decrease the thickness.

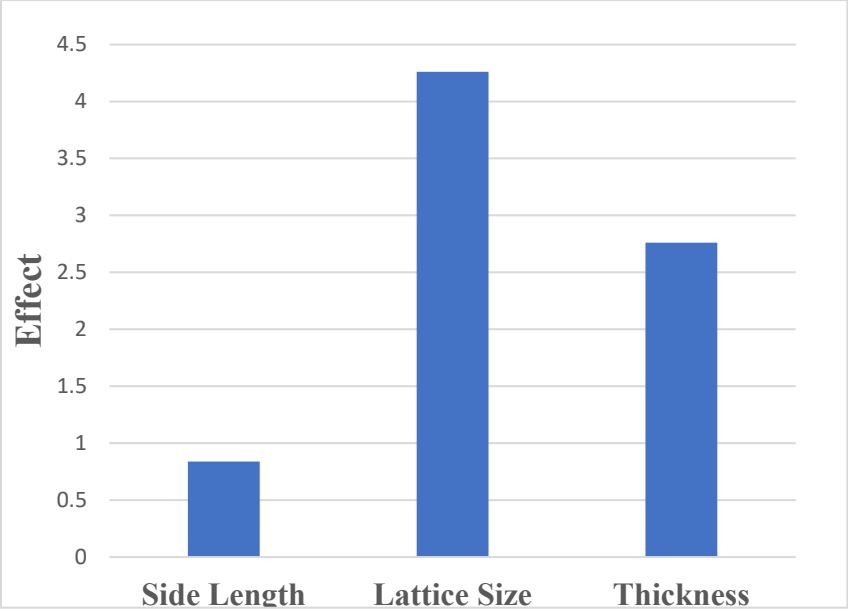

Fig 11. The input parameters' effects on the bandgap magnitude.

V.Conclusions

The unit cell has been modelled using a COMSOL finite element analysis model based on the parameter setups for its wave vector dispersion curves and their frequency band structures which have been verified by the results of other literature simulations. The COMSOL finite element analysis model has been validated by the simulation models of the other literature. The wave vector dispersion curves of the unit cell and the maximum bandgap magnitude can be accurately simulated from varying variables such as the side length, the lattice constant, and thickness. The validated simulation model has been applied to develop the response surface method parameter regression model for sensitivity analysis of the input parameters and their interactions. The response surface method parameter regression model is also used for parameter design optimization of the unit cell to achieve the largest bandgap magnitude. Three geometrical parameters of the gap radius, lattice constant, and thickness are selected and arranged according to the central composite design. Based on the 16 sets of the COMSOL simulation runs from the input parameter combinations of the CCD design, the response target results of the maximum bandgap magnitude values are obtained. The 16 sets of input parameters of the CCD design and

the corresponding response target results of the maximum bandgap magnitude values are used to fit the response surface method model. The sensitivity analysis results of the maximum bandgap magnitude values to the input parameters and their interactions are quantified from the amplitude of the coefficients of the individual RSM model equation terms. Both the RSM model and its parameter sensitivity analysis have been validated by the ANOVA. The maximum bandgap magnitude results of the RSM regression parameter model have also been verified by those of the COMSOL simulation model. The RSM regression parameter model has indicated that the lattice constant has the largest effect on the bandgap magnitude. The largest bandgap magnitude calculated from the RSM regression parameter model is 16.355 GHz with the parameter combination of the side length of 15.268 nm, the lattice constant of 157.889 nm, and the thickness of 2.933 nm. The optimization results have been verified by those calculated by the COMSOL simulation model from the input parameter combinations arranged by the CCD. Both the RSM model and COMSOL model have predicted a similar maximum bandgap magnitude of 16.34 GHz. Therefore, it can be concluded that the maximum bandgap magnitude of the unit cell has been greatly increased through the input parameter optimization.

VI.References

[1] L. E. Bell, "Cooling, Heating, Generating Power, and Recovering Waste Heat with Thermoelectric Systems," *Science,* vol. 321, no. 5895, pp. 1457-1461, 2008, doi: doi:10.1126/science.1158899.

[2] G. S. Nolas, J. Sharp, and J. Goldsmid, *Thermoelectrics: Basic Principles and New Materials Developments*. Springer Berlin Heidelberg, 2010.

[3] G. J. Snyder and E. S. Toberer, "Complex thermoelectric materials," *Nature Materials,* vol. 7, no. 2, pp. 105-114, 2008/02/01 2008, doi: 10.1038/nmat2090.

[4] S. Narayana and Y. Sato, "Heat Flux Manipulation with Engineered Thermal Materials," *[prl] Physical Review Letters 108 21, p. 214303, 05/21/ 2012, doi: 10.1103/Phys. Rev. Lett.108.214303*

[5] J.-K. Yu, S. Mitrovic, D. Tham, J. Varghese, and J. R. Heath, "Reduction of thermal conductivity in phononic nanomesh structures," *Nature Nanotechnology,* vol. 5, no. 10, pp. 718-721, 2010/10/01 2010, doi: 10.1038/nnano.2010.149.

[6] J. Maire, R. Anufriev, R. Yanagisawa, A. Ramiere, S. Volz, and M. Nomura, "Heat conduction tuning by wave nature of phonons," (in eng), *Sci Adv,* vol. 3, no. 8, pp. e1700027-e1700027, 2017, doi: 10.1126/sciadv.1700027.

[7] J. Vondřejc, E. Rohan, and J. Heczko, "Shape optimization of phononic band gap structures using the homogenization approach," *International Journal of Solids and Structures,* vol. 113-114, pp. 147-168, 2017/05/15/ 2017, doi: https://doi.org/10.1016/j.ijsolstr.2017.01.038.

[8] T. D. Ngo, A. Kashani, G. Imbalzano, K. T. Q. Nguyen, and D. Hui, "Additive manufacturing (3D printing): A review of materials, methods, applications and challenges," *Composites Part B: Engineering,* vol. 143, pp. 172-196, 2018/06/15/ 2018, doi: https://doi.org/10.1016/j.compositesb.2018.02.012.

[9] O. Vizuete, "Simulation study of phononic crystal structures," ed, 2017.

[10] T. Guo *et al.*, "Anisotropic phononic crystal structure with low-frequency bandgap and heat flux manipulation," *Science China Physics, Mechanics & Astronomy,* vol. 63, no. 2, p. 224711, 2019/08/29 2019, doi: 10.1007/s11433-019-9437-x.

[11] A. Shelke, S. Banerjee, A. Habib, E. K. Rahani, R. Ahmed, and T. Kundu, "Wave guiding and wave modulation using phononic crystal defects," *Journal of Intelligent Material Systems and Structures,* vol. 25, no. 13, pp. 1541-1552, 2014, doi: 10.1177/1045389x13507344.

[12] D. P. Elford, "Band gap formation in acoustically resonant phononic crystals," Loughborough University, 2010. [Online]. Available: https://repository.lboro.ac.uk/articles/thesis/Band_gap_formation_in_acoustically_resonant_phononic_crystals/9410123

[13] F. Warmuth, M. Wormser, and C. Körner, "Single phase 3D phononic band gap material," (in eng), *Sci Rep,* vol. 7, no. 1, pp. 3843-3843, 2017, doi: 10.1038/s41598-017-04235-1.

[14] C. Hakoda, J. Rose, P. Shokouhi, and C. Lissenden, "Using Floquet periodicity to easily calculate dispersion curves and wave structures of homogeneous waveguides," *AIP Conference Proceedings,* vol. 1949, no. 1, p. 020016, 2018, doi: 10.1063/1.5031513.

[15] L. Peng, J. Bai, X. Zeng, and Y. Zhou, "Comparison of isotropic and orthotropic material property assignments on femoral finite element models under two loading conditions," (in eng), *Medical engineering & physics,* vol. 28, no. 3, pp. 227-33, Apr 2006, doi: 10.1016/j.medengphy.2005.06.003.

[16] E. Holzbecher and H. Si, "Accuracy Tests for COMSOL - and Delaunay Meshes," 2008.

[17] X. Huang, Y. Lai, Z. H. Hang, H. Zheng, and C. T. Chan, "Dirac cones induced by accidental degeneracy in photonic crystals and zero-refractive-index materials," *Nature Materials,* vol. 10, no. 8, pp. 582-586, 2011/08/01 2011, doi: 10.1038/nmat3030.

[18] O. Vizuete, "Simulation study of phononic crystal structures," 17003 Student thesis, UPTEC Q, 2017. [Online]. Available: http://urn.kb.se/resolve?urn=urn:nbn:se:uu:diva-326118

[19] M. S. Kushwaha, B. Djafari‐Rouhani, L. Dobrzynski, and J. O. Vasseur, "Sonic stop bands for cubic arrays of rigid inclusions in air," *The Journal of the Acoustical Society of America,* vol. 104, no. 3, pp. 1745-1745, 1998, doi: 10.1121/1.423644.

[20] S. Greenland *et al.*, "Statistical tests, P values, confidence intervals, and power: a guide to misinterpretations," (in eng), *Eur J Epidemiol,* vol. 31, no. 4, pp. 337-350, 2016, doi: 10.1007/s10654-016-0149-3.

Appendix 1: Band gap figures

Run1

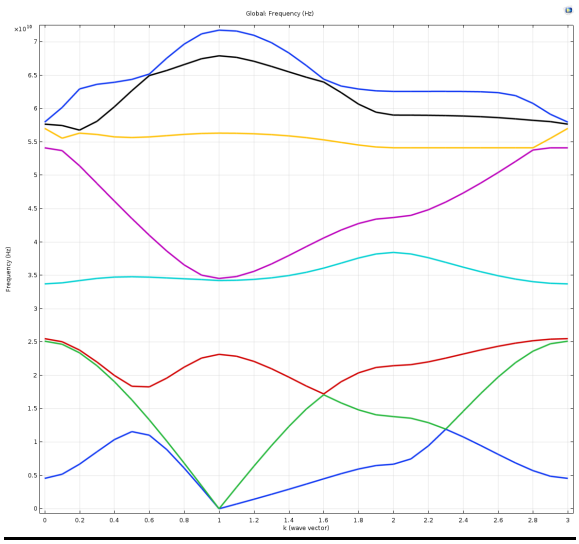

Run2

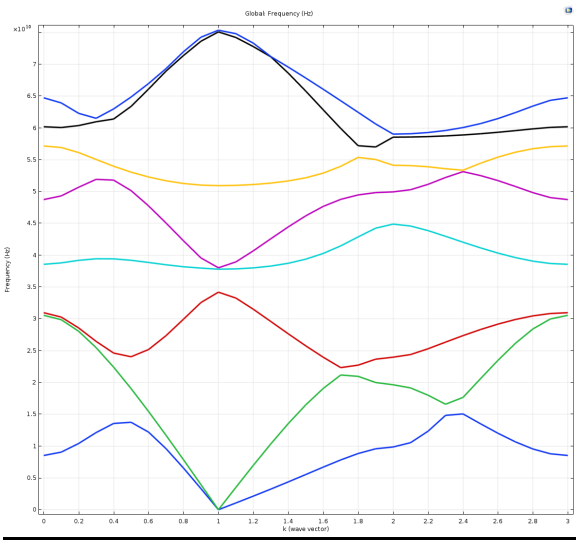

Run3

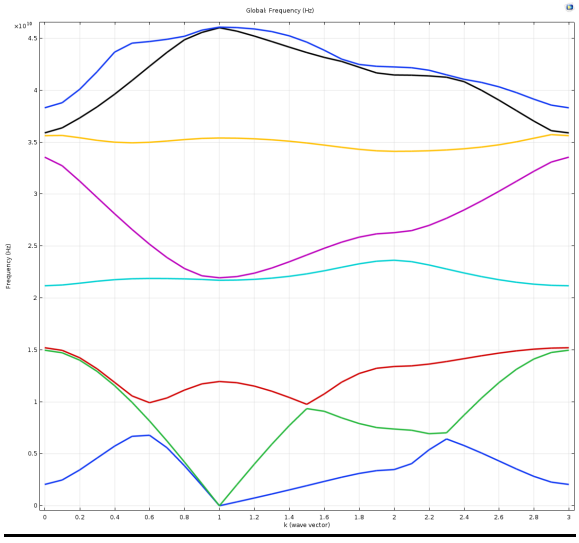

Run4

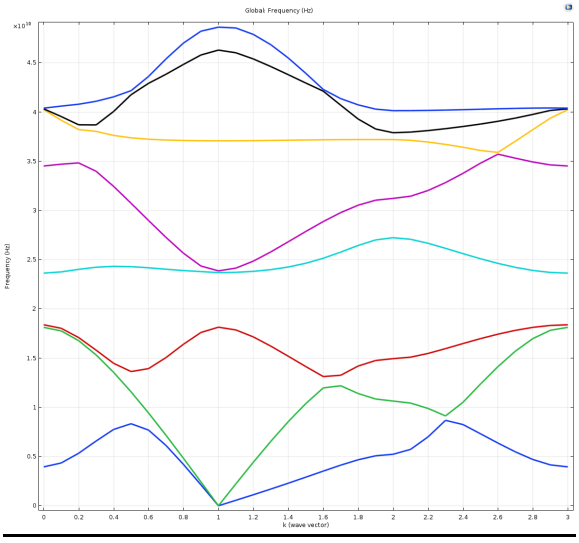

Run5

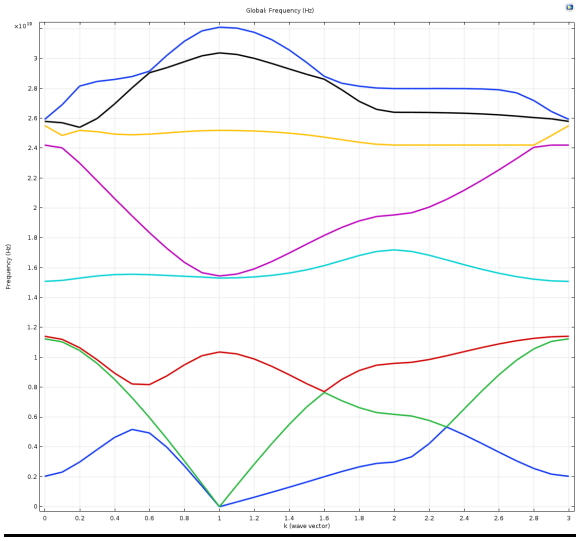

Run6

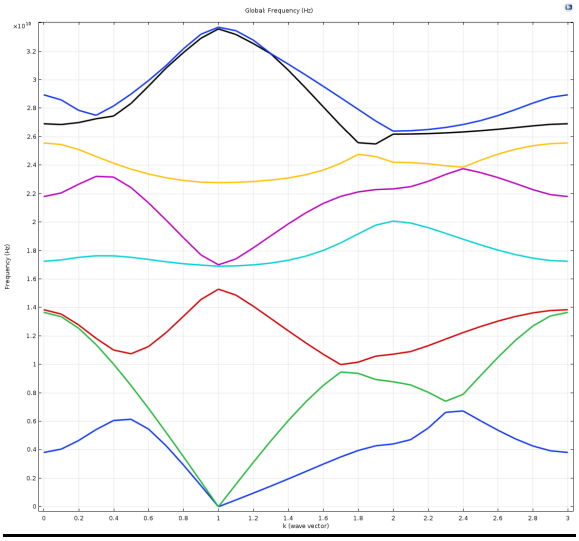

Run7

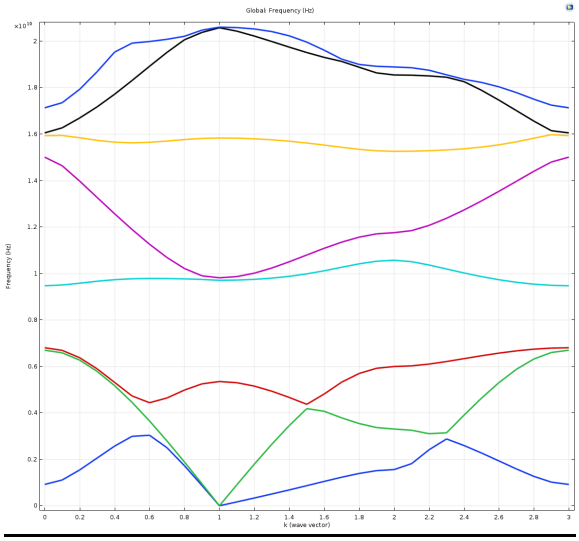

Run8

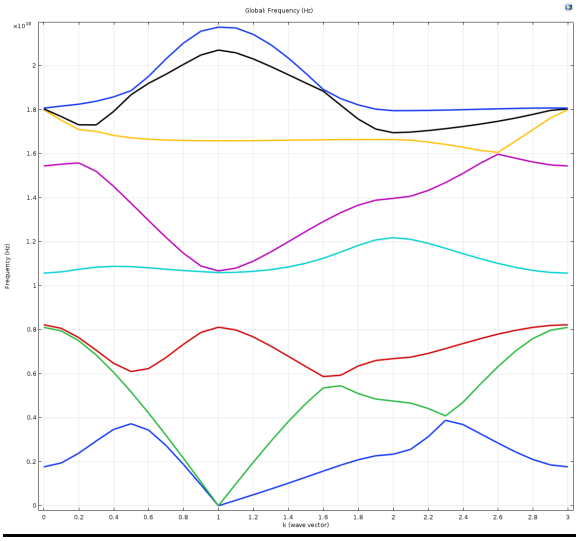

Run9

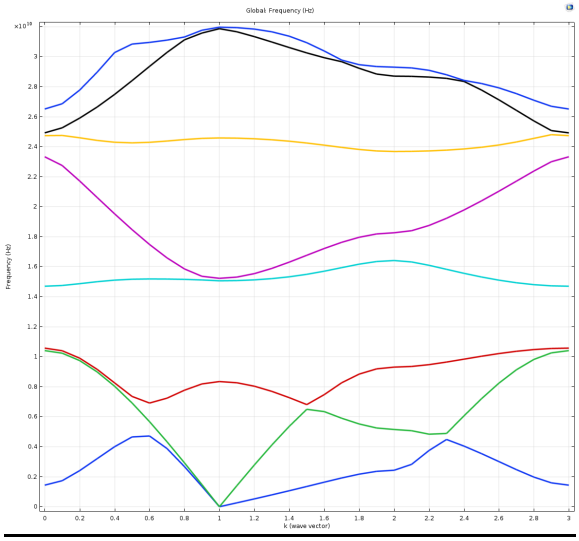

Run10

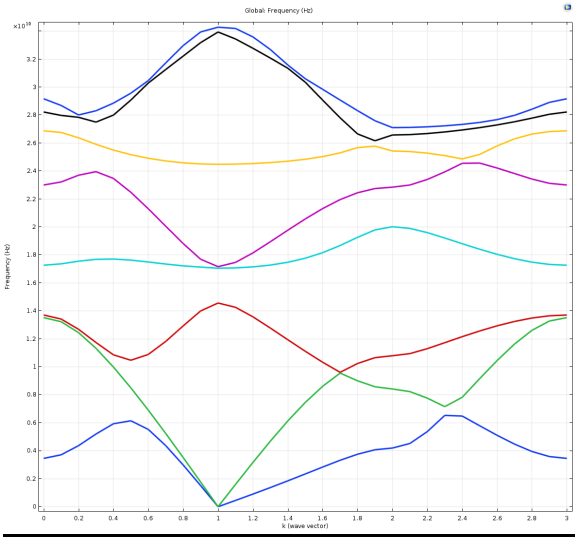

Run11

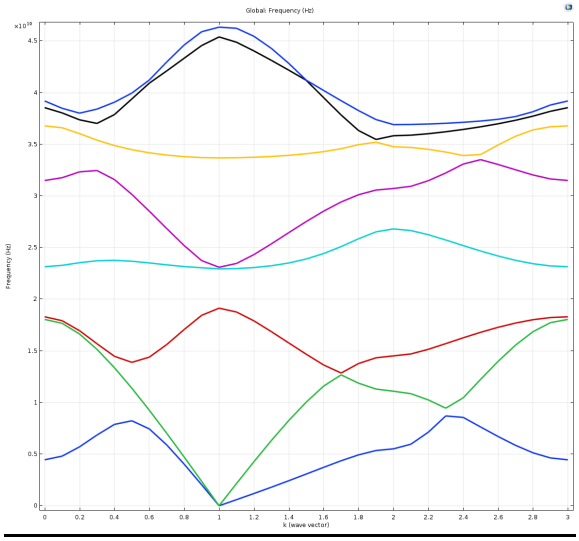

Run12

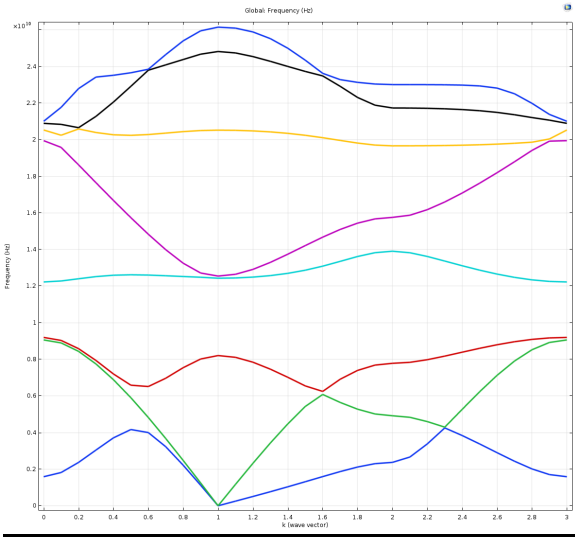

Run13

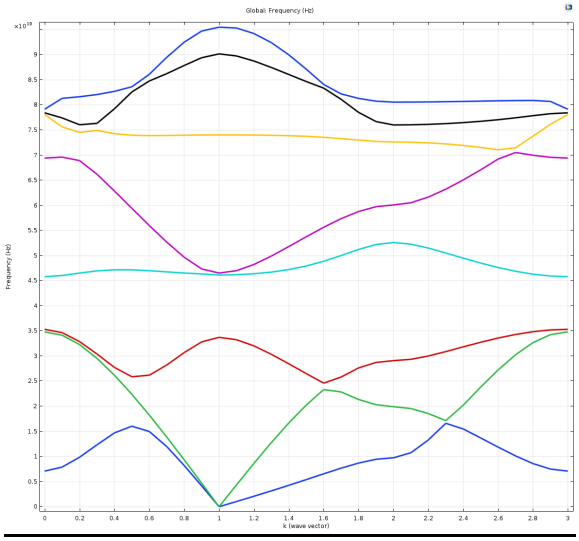

Run14

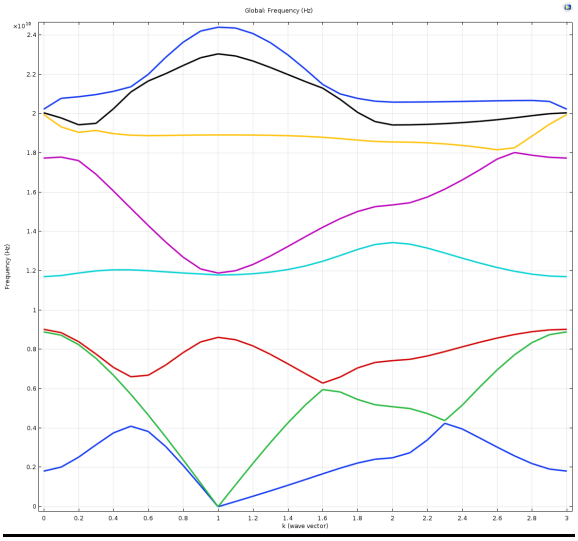

Run15

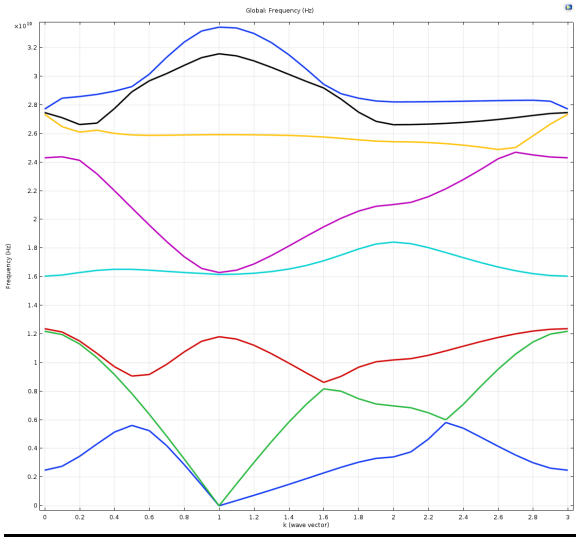

Run16